STATIC AND CYCLIC LOAD TESTS ON MODEL GROUTED PILES IN MARINE CALCAREOUS SEDIMENTS

by

C.Y. Lee[1] and H.G. Poulos[2]

ABSTRACT

Two series of model pile tests have been carried out in a specially-designed apparatus to investigate the characteristics of skin friction on grouted piles in an offshore calcareous sand.

The first series of tests has investigated the influence of overburden pressure and relative density on static friction and soil modulus, and the degradation of skin friction under displacement-controlled cyclic loading. It has been found that very severe degradation can occur if the cyclic displacement amplitude exceeds the displacement required to cause slip of the pile under static loading.

The second series of tests has investigated the stability of the pile under various combinations of mean and cyclic load levels. On a cyclic stability diagram plotting cyclic load level against mean load level, two distinct zones have been identified, a stable zone in which cyclic loading has no effect on pile capacity, and an unstable zone in which cyclic loading causes the pile to fail within a specified number of cycles.

These cyclic stability characteristics have been compared with some field test results and found to be consistent over a wide range of load levels.

A theoretical analysis based on a simple degradation model is described, and is shown to predict the general behaviour of the model pile tests reasonably well.

INTRODUCTION

Driven piles and grouted piles are very commonly used in offshore foundations. Due to significant economy in installation procedures and time, the former is preferred whenever possible. However it is known that the skin friction of driven piles in offshore calcareous soils is low mainly due to low lateral soil pressures caused by pile driving (Lu, 1986; Murff, 1987; Nauroy et al, 1985a, 1985b; Poulos et al, 1986). In the same calcareous soils, some field and laboratory tests have indicated that the static skin friction of grouted piles can be as much as seven times higher than

---

[1] Research Fellow, School of Civil and Mining Engineering, University of Sydney, Australia.

[2] Professor of Civil Engineering, School of Civil and Mining Engineering, University of Sydney, Sydney, 2006, Australia.

for driven piles. However a limited number of tests have also indicated that cyclic loading can significantly reduce the skin friction developed on grouted piles (Murff, 1987; Nauroy et al, 1985a, 1985b).

This paper describes model pile tests which have been carried out in a specially-designed apparatus to investigate the skin friction of grouted piles in an offshore calcareous sand. The influence of overburden pressure, relative density and over-consolidation ratio on the static skin friction and soil modulus is illustrated. The major objective of the tests has been to examine the degradation of skin friction and the stability of the pile under cyclic loading. Comparisons between these model test and some field test results are also presented and discussed. Finally a theoretical analysis of cyclic response, based on a simple degradation model, is described and the theoretical response is compared with the behaviour observed from laboratory tests. It should be noted that most of the displacement-controlled and load-controlled test results have been published separately in the previous two papers (Poulos and Lee 1988, 1989) however the writers believe that it is useful to present them together in this paper.

SOIL CHARACTERISTICS

The soil used in the model pile tests was obtained from the North-West of Australia at the site of the North Rankin A platform. The grading curve for this soil is shown in Fig. 1, and it is seen to consist primarily of particles of silt and sand size. The minimum and maximum densities of the sand were about 1.05 t/m³ and 1.37 t/m³ respectively. The average carbonate content is 97%. Drained triaxial compression tests have shown that the drained properties of the sand can be approximated as follows (Hull et al, 1988) :

$$\phi' = 46.8 - 0.02 \sigma_c' \tag{1}$$

$$E_{max}' = 7.8 + 0.32 \sigma_c' \tag{2}$$

in which ϕ' is the drained peak friction angle, E_{max}' is the drained Young's modulus in MPa at a low strain level, and σ_c' is the effective confining pressure in the range of 100 to 400 kPa. The drained Poisson's ratio, v_{min}', at low strain level is found to be insensitive to the deviatoric stress level, with an average value of about 0.15.

LABORATORY APPARATUS AND TEST PROCEDURE

The apparatus is shown diagrammatically in Fig. 2. The internal diameter of the vessel was 180 mm and the depth 256 mm. This device was specially developed to allow the pile shaft to be installed in a soil layer which had stress-controlled end conditions, with an equal consolidation pressure being applied to both the top and bottom of the soil sample, and the sides being restrained. Consolidation is thus carried out under confined one-dimensional conditions. Poulos and Chan (1986) have described this device in more detail.
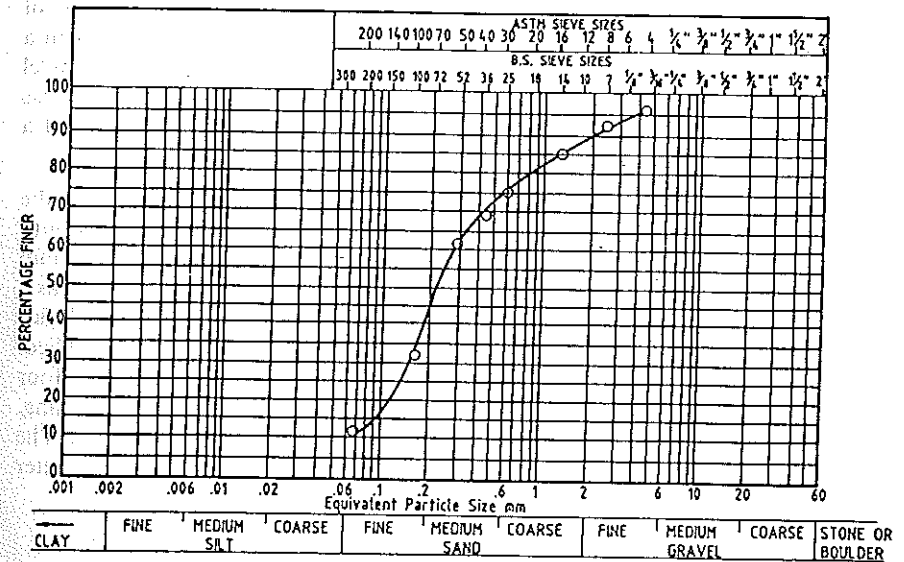

Fig. 1 Grading Curve of North Rankin Soil.

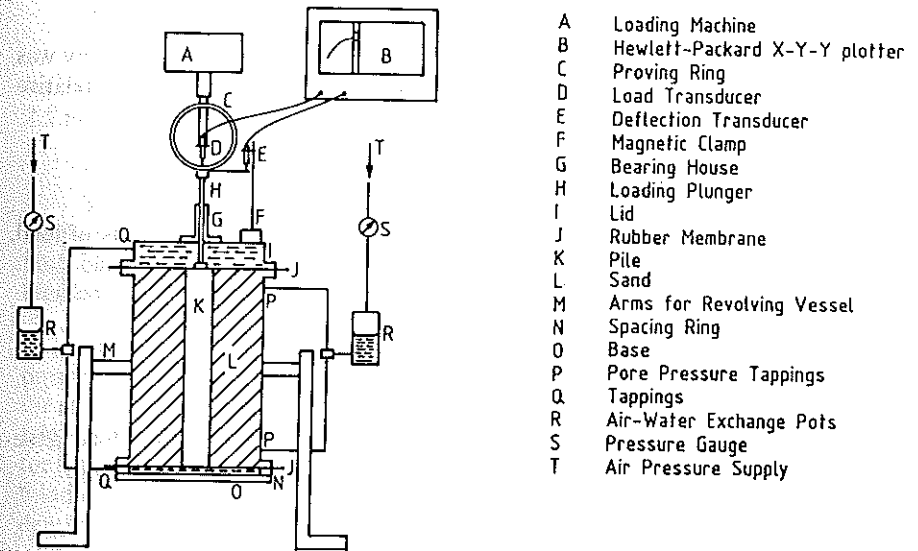|	
A	Loading Machine
B	Hewlett-Packard X-Y-Y plotter
C	Proving Ring
D	Load Transducer
E	Deflection Transducer
F	Magnetic Clamp
G	Bearing House
H	Loading Plunger
I	Lid
J	Rubber Membrane
K	Pile
L	Sand
M	Arms for Revolving Vessel
N	Spacing Ring
O	Base
P	Pore Pressure Tappings
Q	Tappings
R	Air-Water Exchange Pots
S	Pressure Gauge
T	Air Pressure Supply

Fig. 2 Experimental Apparatus.

The soil was rained into the vessel and then saturated by an upward flow of water. The saturated soil was initially consolidated prior to pile installation with a presssure equal to the final test overburden presssure. In constructing the model grouted piles, a metal drill of about 22.2 mm diameter attached to a long handle was used as an auger to bore a hole to the bottom of the sand bed, with the aid of a guiding device. The hole was found to stand open without support.

The sand/cement (type B) and water/cement ratios used in constructing the grouted piles were about 1.2 and 0.5 respectively. The wet cement was poured into the hole using a plastic funnel and then rodded. A metal central rod of about 5 mm diameter with a threaded hole at the top was inserted into the grouted pile to act as a reinforcement and also to provide a connection to the loading plunger. The device was immediately re-assembled and the required overburden pressure then re-applied. The grouted pile was then allowed to cure under these conditions for at least four days (giving an average grout compressive strength of about 6 MPa) before testing. The dimensions of the grouted pile were measured at the completion of the test. The length of the grouted pile was typically about 256 mm while the average diameter was about 24 mm.

The procedure for the displacement-controlled tests involved three stages :

(i)   an initial static loading test to failure; this stage was terminated after a displacement of 2.5 mm had been reached;

(ii) one and two-way cyclic loading, between pre-determined limits of displacement, for a specified number of cycles;

(iii) a final static loading test to failure.

The ratio of the final load capacity to the initial peak static load capacity was taken to be the degradation factor for skin friction, and was a measure of the relative amount of skin friction remaining after cyclic loading.

For the load-controlled tests, the procedure was as follows :

(i)   an initial static loading to the specified mean load;

(ii) one and two-way cycling loading, between predetermined limits of load, for a specified number of cycles;

(iii) a final static loading test to failure (only for some tests).

EXPERIMENTAL RESULTS

(a) Displacement-controlled Tests

Table 1 summarises the tests carried out, while Fig. 3 shows typical load settlement curves for the grouted model pile under both static and cyclic loadings.

It will be observed from Fig. 3 that :

(i)   the initial static load-settlement curve is highly nonlinear but does not exhibit "strain-softening" behaviour,
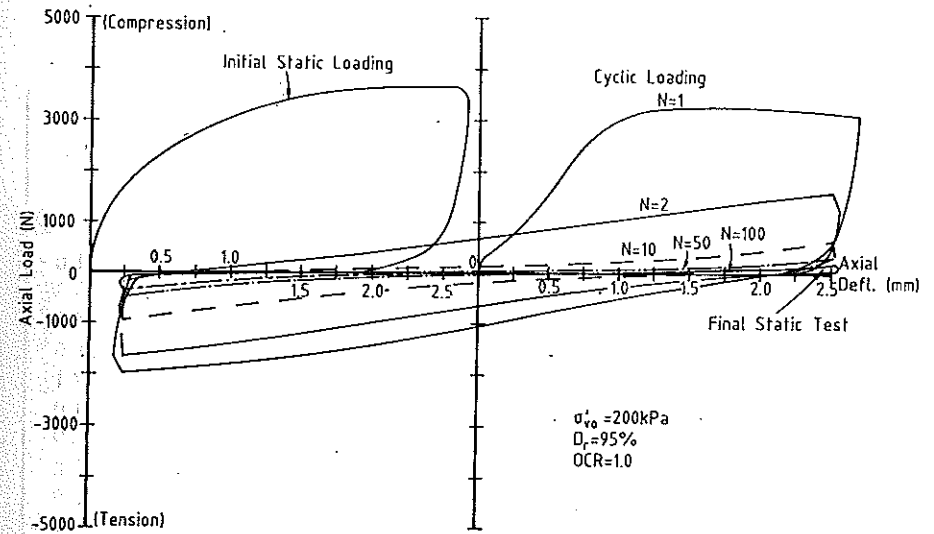
Fig. 3   Typical Test Result for Grouted Pile Shaft.

(ii) cyclic loading, with a displacement amplitude of ± 2.5 mm (10% of diameter) causes a major reduction in load capacity,

(iii) the post-cyclic load capacity is very small.

The behaviour under static and cyclic loading will be discussed in more detail below. The skin friction was calculated as the pile load capacity (at a displacement of 2.5 mm) divided by the surface area of the pile shaft.

Behaviour under Static Conditions

The influence of the effective overburden pressure on the skin friction, f_s, in medium dense sand and dense sand is demonstrated in Fig. 4. The skin friction in both cases increases with increasing effective overburden pressure but tends to a limiting value at higher pressures.

The normalised skin friction, f_s/σ'_{vo}, where σ'_{vo} is the initial effective overburden pressure, increases with increasing over-consolidation ratio, OCR, as shown in Fig. 5 for medium dense sand. For normally consolidated medium dense sand, the value of f_s/σ'_{vo} is about 0.75, which is extremely large in comparison to corresponding values for jacked piles, which can be of the order of 0.05-0.1 (Poulos and Chan, 1986). Fig. 6 indicates that the normalised skin friction also increases with increasing relative density, D_r.

The values of drained Young's modulus E'_{50} of the soil, for a load level of 50% of the ultimate, were backfigured from the load-settlement curves, using the elastic

Table 1 Summary of Displacement-Controlled Tests.

Test	D_r %	σ'_{vo} kPa	OCR	E'_{50} MPa	f_s kPa	No.of Cycles N	$\pm P_c/d$	f_c kPa
1	55	200	1.0	23.7	130.9	10	0.02	141.6
2	55	200	1.0	24.6	133.9	100	0.10	8.3
3	60	200	1.0	22.8	147.1	100	0.02	114.3
4	59	200	1.0	22.6	133.3	100	0.04	58.6
5	60	200	1.0	17.9	152.0	100	0.01	172.1
6	62	400	1.0	38.9	196.8	100	0.10	1.0
6A	58	100	1.0	11.4	80.0	100	0.02	83.9
7A	61	400	1.0	32.5	232.0	100	0.02	172.8
8	80	200	1.0	19.7	160.6	100	0.02	122.9
9	60	66.7	3.0	19.8	93.5	100	0.02	43.9
10	60	33.3	6.0	14.0	70.4	100	0.02	44.8
11	95	100	1.0	9.9	109.8	100	0.02	95.1
13	95	200	1.0	21.2	222.3	100	0.02	160.3
14	95	200	1.0	24.9	202.5	100	0.04	68.2
15	95	200	1.0	21.6	190.2	100	0.10	9.2
16	95	200	1.0	21.5	218.8	100	0.01	208.1
17	96	400	1.0	35.5	256.0	100	0.02	160.0
42	61	200	1.0	24.3	159.6	50	0.02	141.5
43	61	200	1.0	25.0	130.1	50	0.04	75.1
44	62	200	1.0	21.5	142.8	10	0.04	109.5
45	58	200	1.0	20.0	141.7	500	0.04	63.4

analysis of Randolph and Wroth (1978). Fig. 7 shows that E'_{50} increases with increasing effective overburden pressure in both medium dense sand and dense sand. It seems that the relative density of the soil has little influence on E'_{50}. Fig. 8 plots E'_{50}/σ'_{vo} versus OCR, and demonstrates that this ratio increases with increasing OCR. For normally consolidated soil, the ratio E'_{50}/σ'_{vo} is about 100, rising to over 400 for an OCR of 6.

Behaviour under Cyclic Loading

The degradation factor for skin friction, D_τ, is defined as the ratio of ultimate skin friction following cyclic loading, f_c, to static skin friction f_s, D_τ is found to depend on the magnitude of cyclic displacement $\pm P_c$. For N = 100 cycles, Fig. 9 shows the variation of D_τ with cyclic displacement, $\pm P_c$, in both medium dense sand and
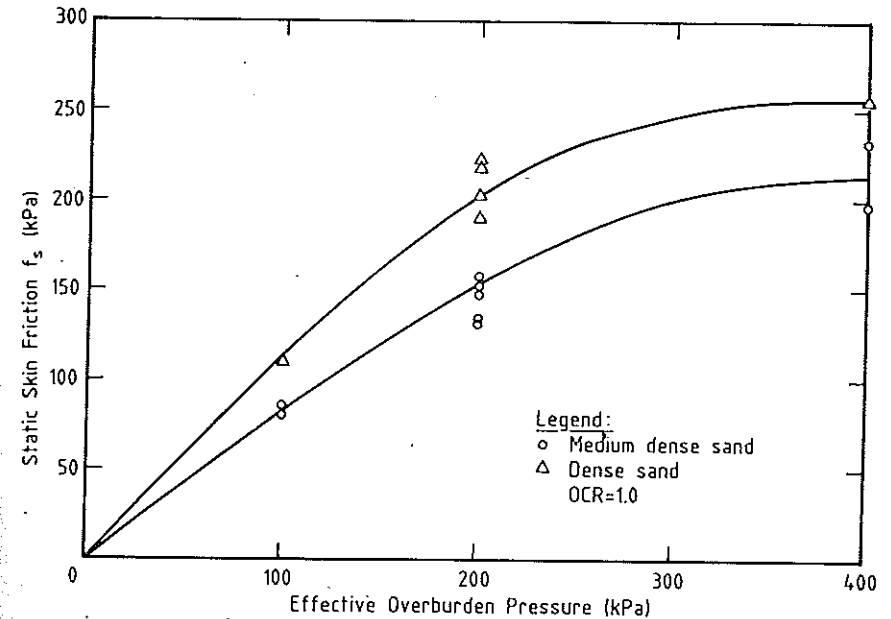

Fig. 4 Influence of Effective Overburden Pressure on Static Skin Friction.
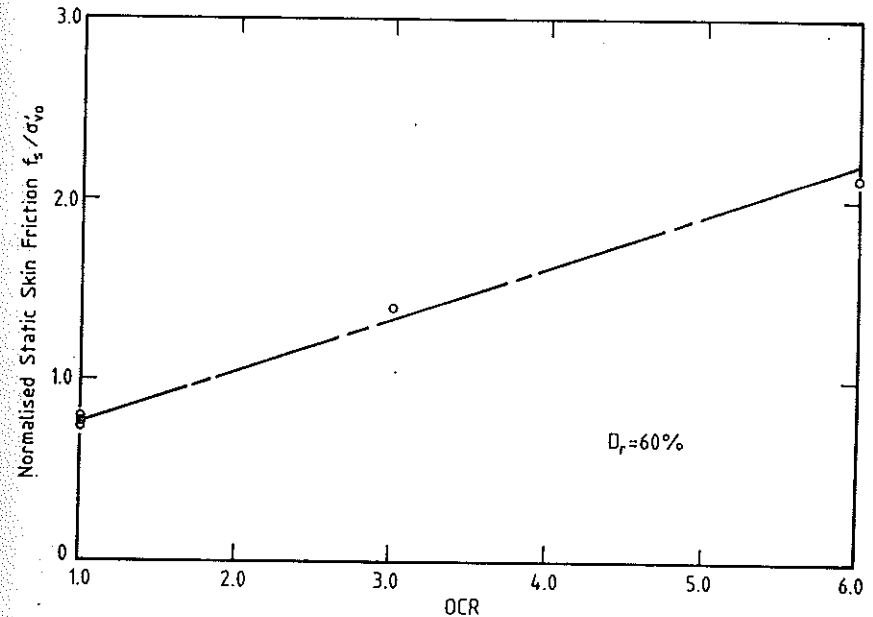

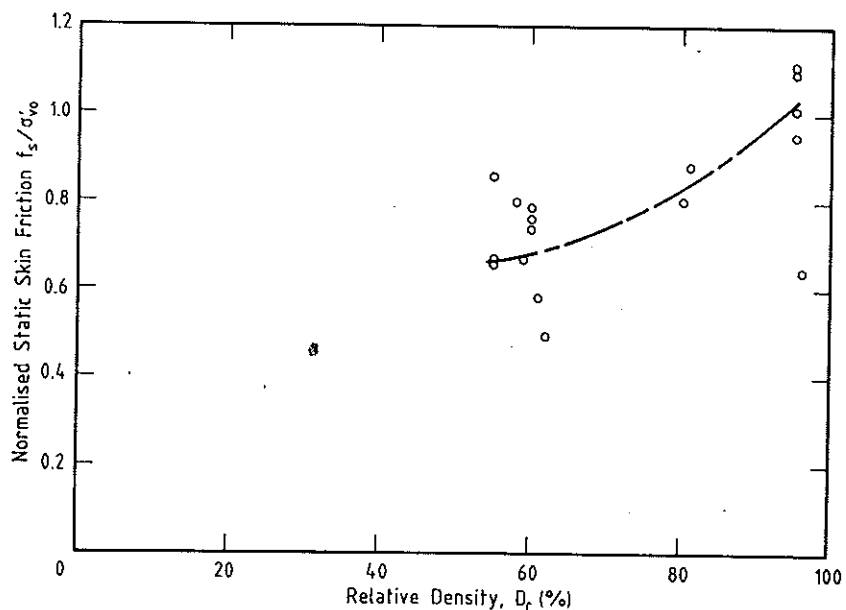**Fig. 5 Effect of OCR on Normalised Skin Friction.**

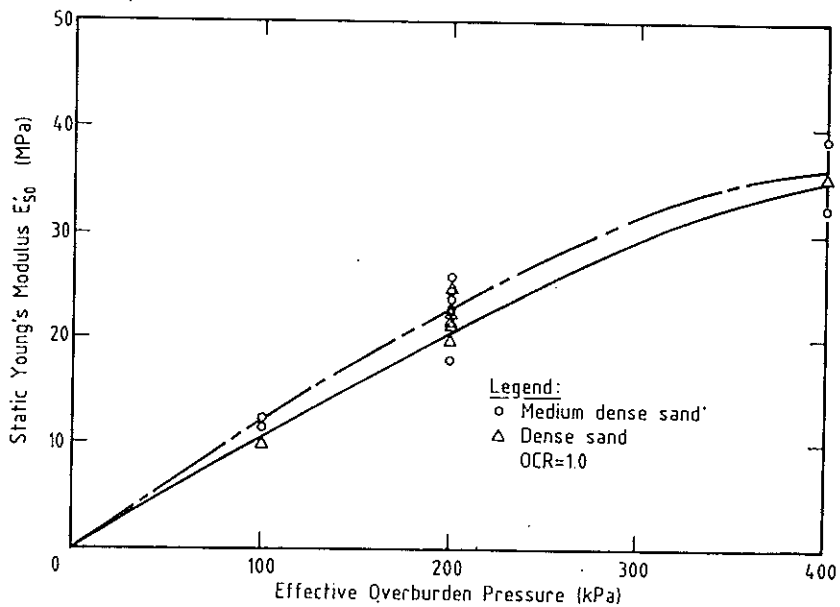Fig. 6   Influence of Relative Density on Normalised Static Skin Friction.

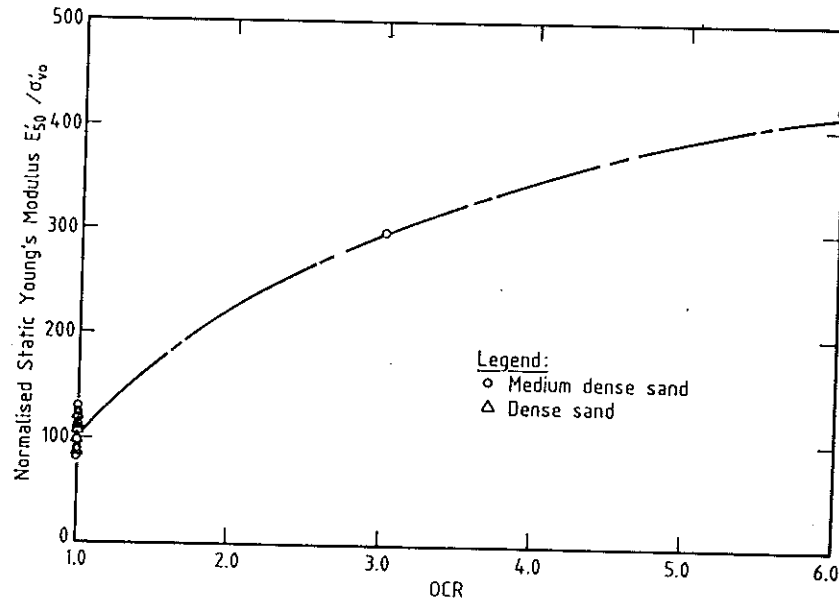Fig. 7   Influence of Effective Overburden Pressure on Static Young's Modulus.

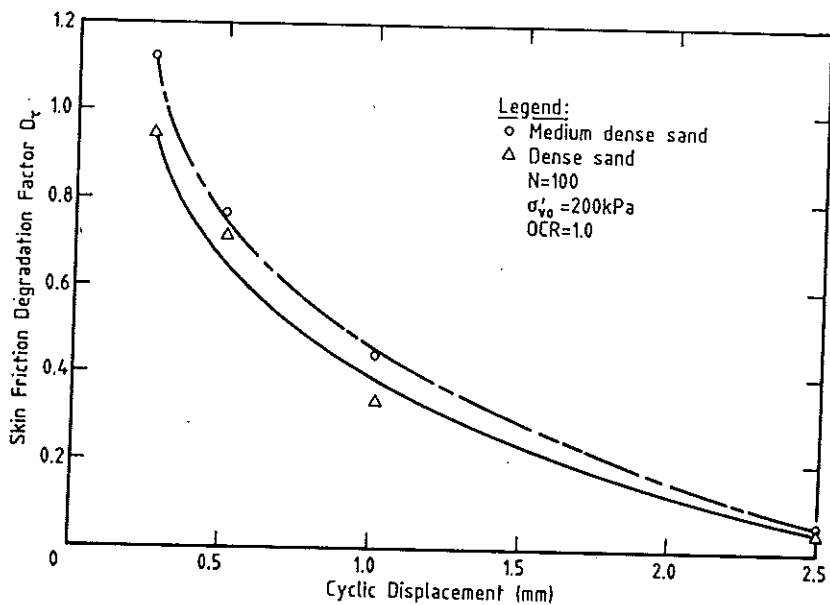Fig. 8 Influence of OCR on Normalised Static Young's Modulus.

Fig. 9   Effect of Cyclic Displacement on Skin Friction Degradation Factor.
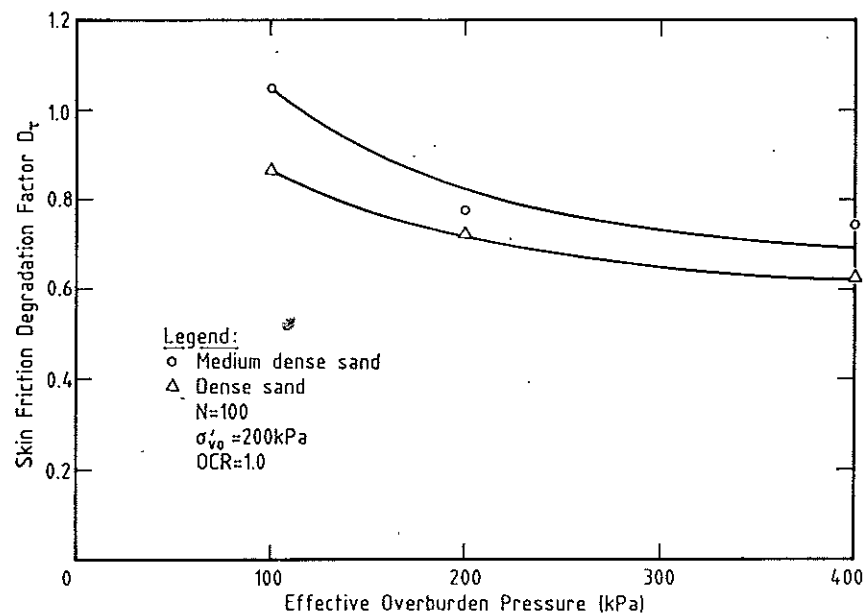
Fig. 10 Influence of Effective Overburden Pressure on Skin Friction Degradation Factor-Cyclic Displacement = ± 0.5 mm.

dense sand. The skin friction degrades more in dense sand than in medium dense sand but the difference decreases with increasing cyclic displacement. At large cyclic displacements, (e.g. ± P_c = 10% of pile diameter), the skin friction after cyclic loading is reduced to about 5% of the initial static value.

The variation of D_τ with effective overburden pressure is plotted on Fig. 10 for both medium dense sand and dense sand. It is found that D_τ decreases with increasing effective overburden pressure for both type of sands, although there appears to be little influence for overburden pressures in excess of 200 kPa. For a given cyclic displacement, both the over-consolidation ratio, OCR, and relative density, D_r, are found to have little influence on cyclic degradation of skin friction.

Fig. 11 shows the variation of degradation factor with the number of cycles, for various cyclic displacement amplitudes. For relatively large cyclic displacements, most of the degradation occurs within the first 50 cycles. For smaller cyclic displacements, there may be an increase in skin friction for small number of cycles, but there also appears to be a subsequent degradation which continues beyond 50 cycles.

Comparison with other Test Data

Data relevant to the cyclic degradation of skin friction of grouted piles in cal-
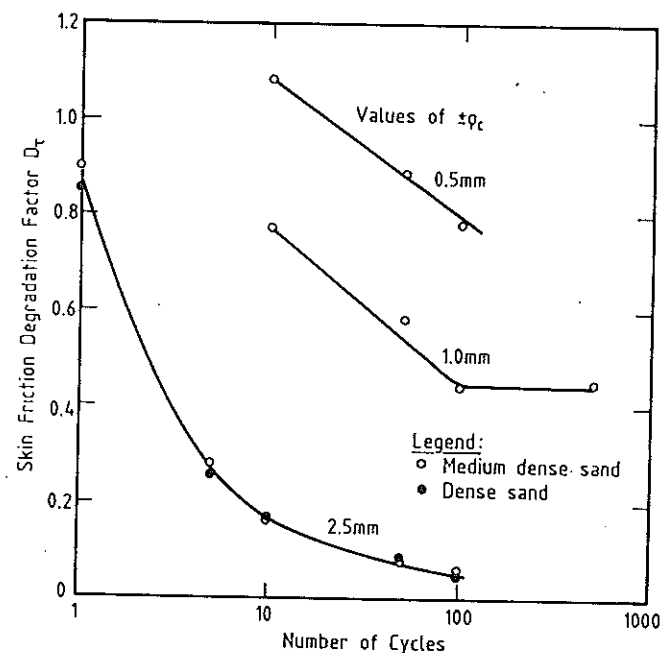
Fig. 11 Variation of Degradation Factor with Number of Cycles.

careous sediments was also available from two other sources :

(i) model tests on piles in Bass Strait carbonate sands (Young, 1983). The apparatus used for these tests was different from that used for the present tests and the soil was also different, having generally coarser particles than the North Rankin soil,

(ii) constant normal stiffness (CNS) tests, carried out on cemented sediment (calcarenite) cores and reported by Johnston et al (1988).

Various attempts were made to reconcile the data from these two test series and from the tests reported herein. It was found that this could be done if the skin friction degradation factor was related to the amplitude of the cyclic slip displacement i.e. the difference between the overall cyclic displacement and the displacement required to develop full slip at the interface under static loading conditions. Fig. 12 plots the relationship between the degradation factor and the cyclic slip displacement and reveals a reasonable degree of consistency in the results of the three types of test.

Fig. 12 has important practical implications as it suggests that :

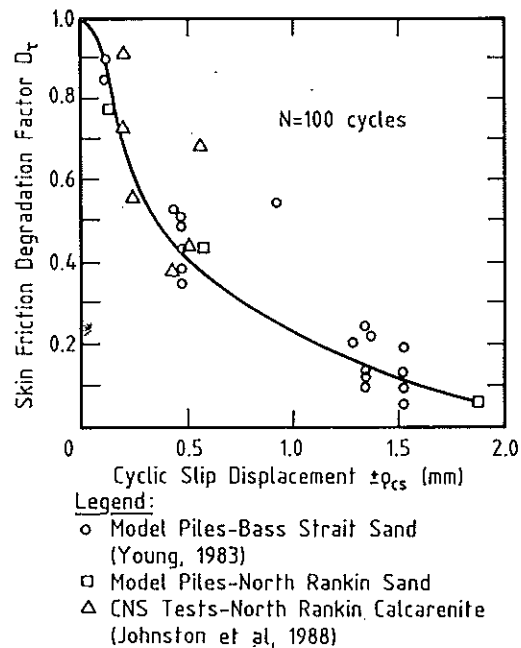(i) degradation of skin friction is controlled by the cyclic slip displacement

Fig. 12 Dependence of Skin Friction Degradation on Cyclic Slip Displacement, Grouted Piles in Calcareous Soils.

(rather than the overall cyclic displacement),

(ii) repeated application of relatively ssmall cyclic slip displacements of the order of 1 to 2 mm can cause very substantial losses in skin friction along model grouted piles in calcareous sediments.

It is also interesting to note that these conclusions provide experimental support for the hypothesis proposed by Matlock and Foo (1979), in which cyclic degradation occurred after a reversal of slip at a point along the pile. This model has been used for the theoretical analysis of grouted pile performance in calcarenite (Poulos, 1988).

(b) Load-controlled Tests

Fig. 13 shows typical load-settlement curves for the model grouted pile under load-controlled testing. The pile was assumed to fail at a permanent displacement of 2.5 mm (i.e. 10% of pile diameter). A summary of the tests carried out at various combinations of mean (P_o) and cyclic ($\pm P_c$) load levels is given in Table 2.

The test results show that the permanent displacement S_p increases with increasing cyclic load level and number of cycles. Fig. 14 shows that S_p can be approxi-
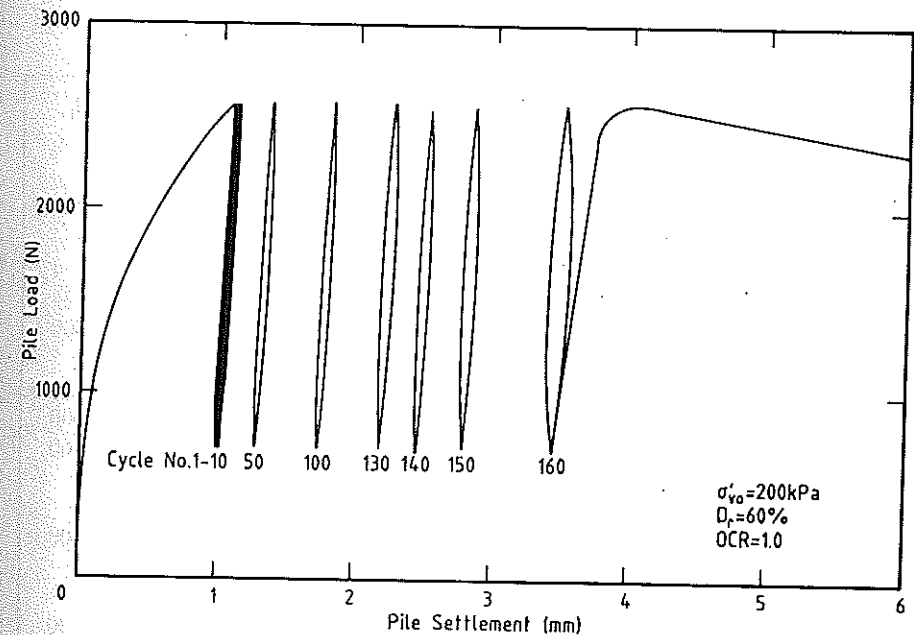
Fig. 13 Typical Load-controlled Model Pile Test.

mately represented by the following expression, which is similar to the form used by Diyaljee and Raymond (1982) for triaxial test results :

$$S_p/d = A \cdot \exp(nX) \cdot N^m \qquad (3)$$

where S_p = permanent displacement
    d = pile diameter
    X = applied cyclic load level
    N = number of cycles
    A, n, m = experimentally-determined parameters.

From the experimental data, average values of $m = 0.28$, $n = 5.1$, and $A = 0.4$ are obtained.

Fig. 15 shows the cyclic stability diagram for the model pile tests. This diagram plots the mean load level against the cyclic load level and indicates the consequent behaviour of the pile.

The following features can be noted :

(i) contours of number of cycles to cause failure are plotted on the diagram. They tend to move closer to each other with increasing mean load levels and also with decreasing cyclic load levels;

Table 2   Summary of Load-Controlled Tests.

TEST No.	D_r	σ'_{vo}	OCR	P_o	P_c	P_{uc}	N_f
					$\pm$		
	%	kPa		P_u	P_u	P_u	
21	60	200	1.0	0.1	0.1	0.97	—
22	60	200	1.0	0.46	0.46	—	4
23	60	200	1.0	0.36	0.36	—	124
24	60	200	1.0	0.27	0.27	—	600
27	59	200	1.0	0.25	0.12	—	—
28A	61	200	1.0	0.6	0.1	—	—
28B	61	200	1.0	0.6	0.2	—	>2000
28C	61	200	1.0	0.6	0.3	—	160
29A	61	200	1.0	0.2	0.1	—	—
29B	61	200	1.0	0.2	0.2	—	—
29C	61	200	1.0	0.2	0.3	—	600
31A	63	200	1.0	0.4	0.1	—	—
31B	63	200	1.0	0.4	0.2	—	—
31C	63	200	1.0	0.4	0.35	0.8	130
32A	58	200	1.0	0.8	0.05	—	—
32B	58	200	1.0	0.8	0.1	—	3000
32C	58	200	1.0	0.8	0.15	0.85	150
33A	59	200	1.0	0	0.2	—	—
33B	59	200	1.0	0	0.4	0.66	130
34B	56	200	1.0	0.9	0.07	—	>2000
36A	56	200	1.0	0.2	0.55	0.73	28
36B	56	200	1.0	0.2	0.7	0.57	2
50	63	200	1.0	0.4	0.6	—	1
51	58	200	1.0	0.8	0.2	—	1
52	59	200	1.0	0.0	0.8	—	2
53	56	200	1.0	0.2	0.4	—	80
54	56	200	1.0	0.2	0.8	—	1
55	59	200	1.0	0.0	0.6	—	14

Fig. 14   Development of Permanent Settlement with Number of Cycles.

(ii)   if the cyclic load level does not exceed about 20% of the static load capacity, P_u, there appears to be no loss of load capacity over a wide range of mean loads. This appears to define the cyclically stable zone;

(iii)   unfortunately, there is no experimental data which can be used to define the metastable zone in which the pile suffers some limited loss of capacity, but does not fail 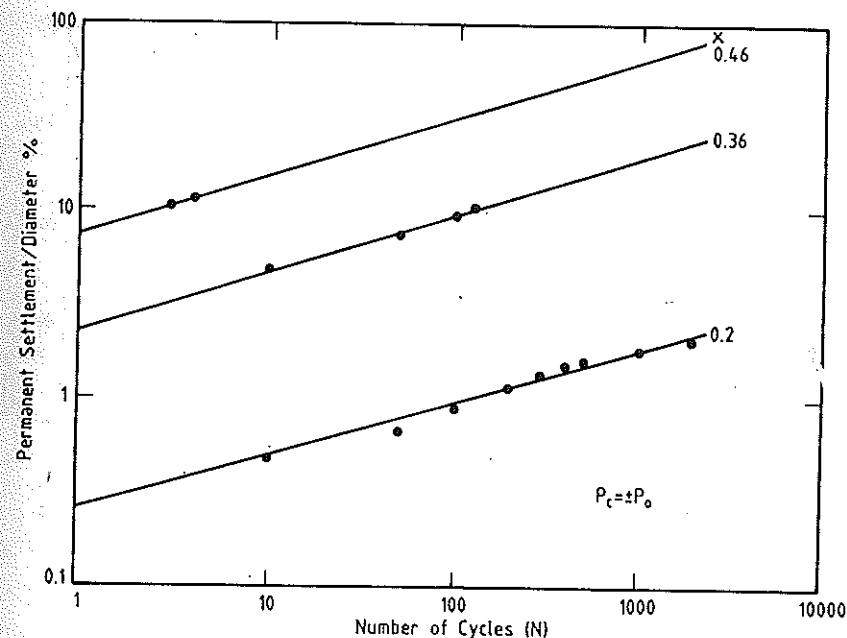during cycling. However, there appears to be a well-defined unstable zone in which cyclic loading results in failure of the pile within a specified number of cycles.

For comparison purposes, some field test results (Deane et al, 1988; Nauroy et al 1985a, 1985b) are also plotted on the cyclic stability diagram and these are found to be consistent with those obtained from the model tests.

"Fatigue curves" which illustrate the relationship between cyclic load level and number of cycles to cause failure, N_f, are shown in Fig. 16. It is found that as the mean load level decreases, the "fatigue curve" tends to become flatter which implies that N_f is very sensitive to cyclic load level.

Fig. 17 demonstrates that the ultimate load capacity after cycling decreases due to cyclic loading. The reduction can be greater than 40% of the static ultimate capacity at high cyclic load levels. For mean load levels in excess of about 46%, failure (or reduction in load capacity), is mostly due to the rapid accumulation of permanent settlement.

THEORETICAL ANALYSIS

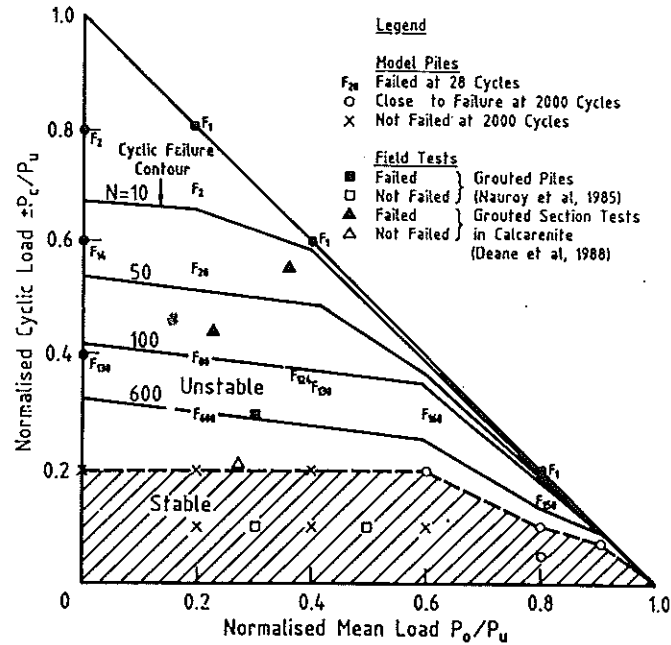Details of an analysis for cyclic axial response are described by Poulos (1989).

Fig. 15 Cyclic Stability Diagram.

Fig. 16 "Fatigue Curves" for Model Piles.

A simplified form of boundary element analysis is used in which the pile is represented as an elastic cylinder and the surrounding soil mass as an elastic continuum. The following features are considered :

(i)   pile-soil slip when the shear stress reaches the current limiting value of shaft resistance;

(ii) accumulation of permanent settlement under cyclic loading; this is described by an expression similar to Equation 3;

(iii) cyclic degradation of shaft resistance; this is expressed by the simple Matlock and Foo (1979) model :

$$D_\tau = (D_\tau - D_{\tau lim}) (1 - \lambda) + D_{\tau lim} \qquad (4)$$

where D_τ = current value of degradation factor
D_τ = degradation factor for previous cycle
$D_{\tau lim}$ = minimum possible degradation factor·
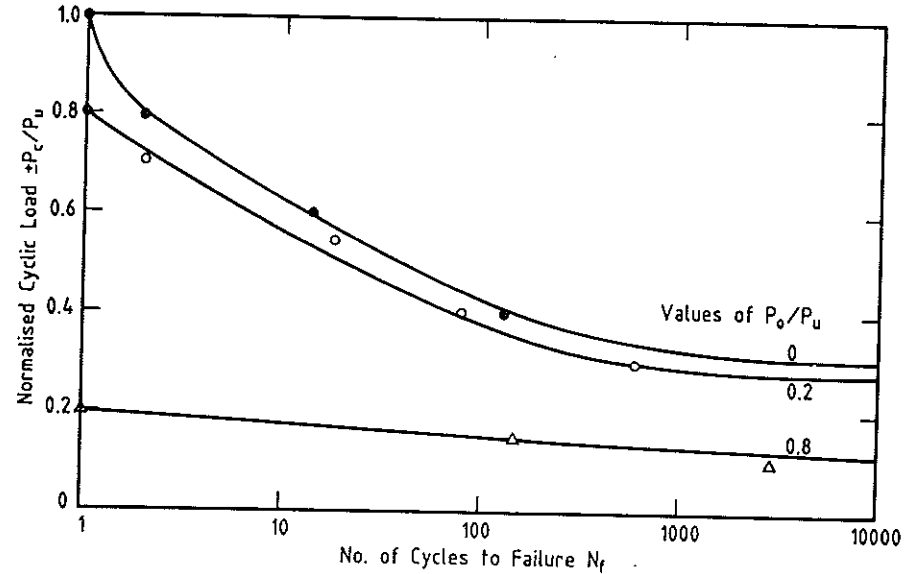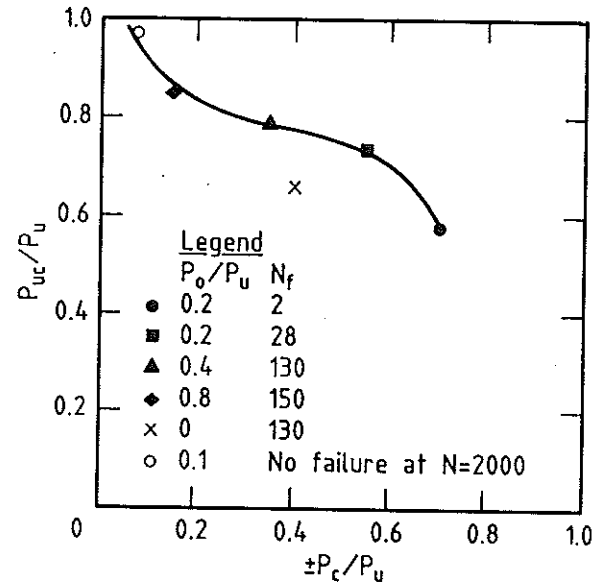λ = degradation rate parameter.

P_{uc} = Ultimate Load after Cycling
N_f = No. of Cycles to Failure

Fig. 17 Effect of Loading on Ultimate Load Capacity.

COMPARISONS BETWEEN SIMPLE ANALYSIS AND MEASURED RESULTS

Fig. 18 illustrates the genertal behaviour of this degradation model for various values of λ. It is found that computed degradation factors, D_τ, using $\lambda = 0.25$ and $D_{\tau lim} = 0.06$, show some limited similarity to those obtained from the model tests.

Table 3 presents the parameters used for the simple analysis of the load-controlled model tests. These parameters have generally been derived from the displacement-controlled model tests, except for the parameters for permanent displacement accumulation.

Fig. 19 compares the computed cyclic stability diagram for the pile subjected to 100 cycles of uniform loading, with that determined from the model tests. Considering the simple form of degradation model, the simple analysis and observed results are in reasonably good agreement.

Fig. 20 demonstrates that the analysis can simulate reasonably well the "fatigue" behaviour of the model piles at various mean load levels. However, Fig. 20 also shows that cyclic degradation can occur at even lower cyclic load levels than the theory predicts. Thus, adequate margins of safety should be used when assessing the possible effects of cyclic loading on grouted pile response.

Table 3   Parameters used for Theoretical Studies.

| Parameters	Definition	Value
E_s	Young's modulus of soil	22 MPa
ν_s	Poisson's ratio of soil	0.35
f_s	limiting static pile shaft resistance	0.13 MPa
$D_{\tau lim}$	limiting shaft resistance degradation factor	0.06
λ	rate factor for shaft resistance degradation	0.25
m	cycle parameter for permanent shaft displacement	0.28
n	stress-level parameter for permanent shaft displacement	5.1
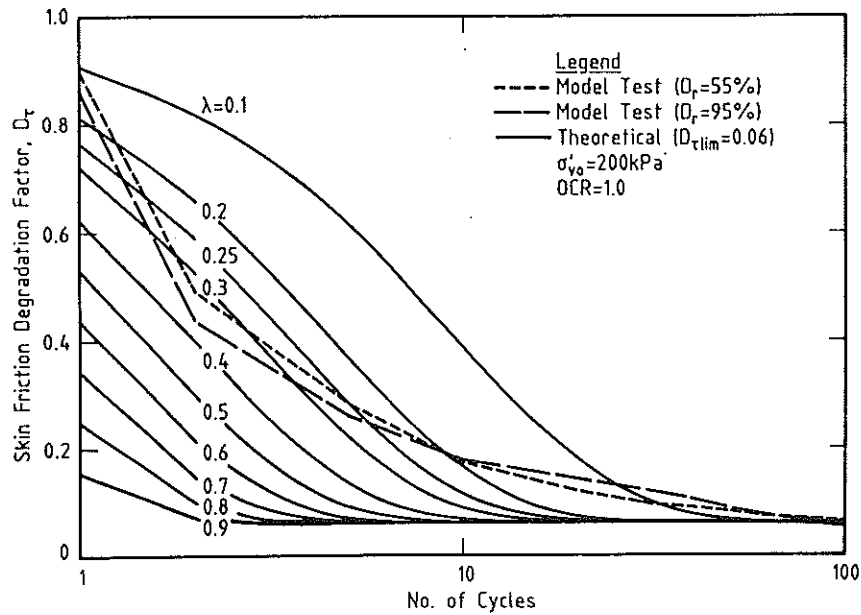
Fig. 18   Comparisons of D_T from Small Model Tests and Reverse-Plastic-Stress Model.
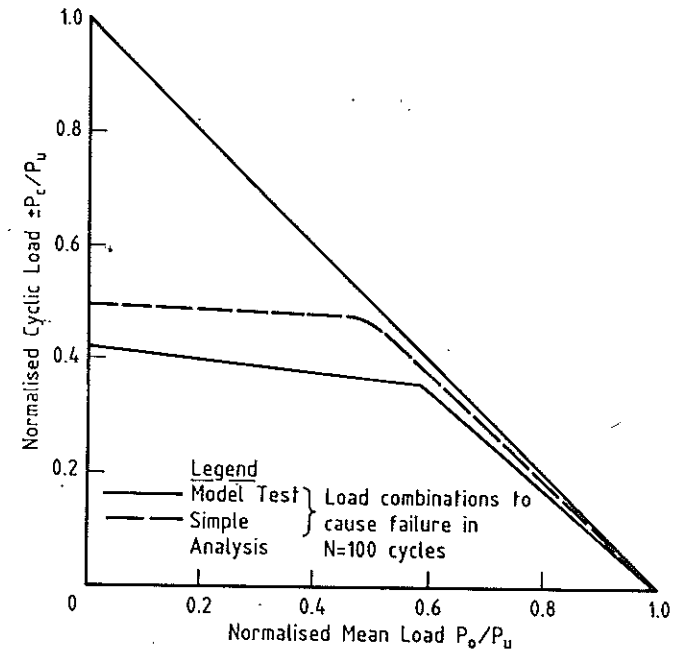

Fig. 19   Comparison Between Cyclic Stability Diagram from Model Tests and Simple Analysis.
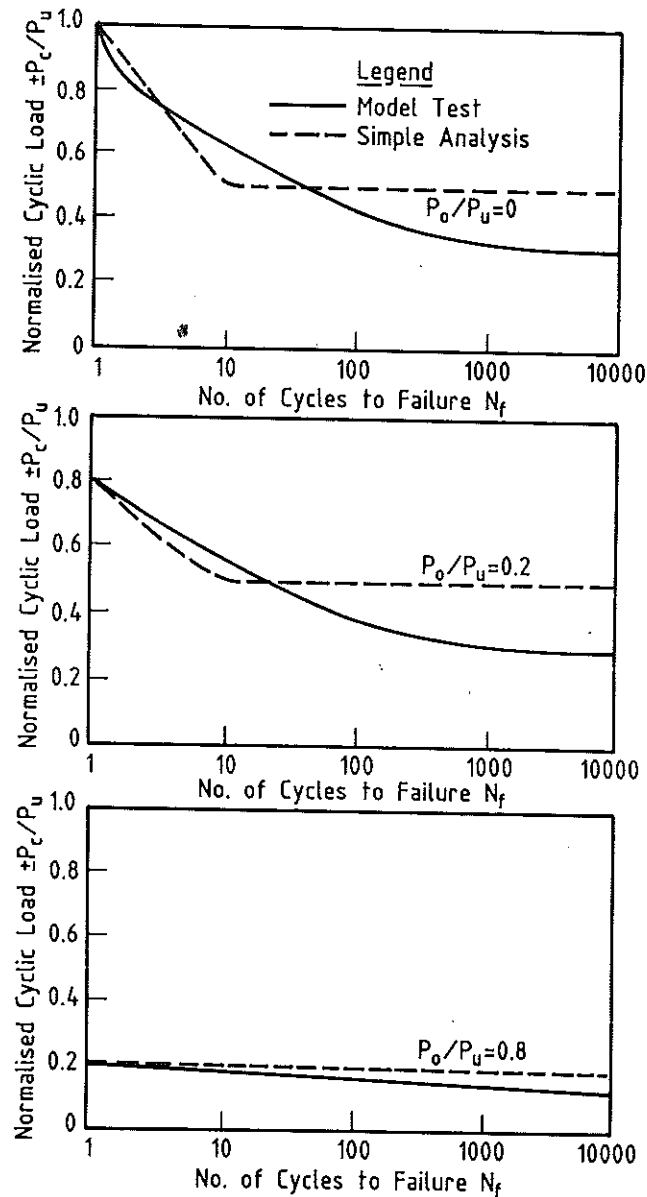
Fig. 20 Comparison Between "Fatigue Curves" in Model Tests and Simple Analysis.

CONCLUSIONS

The tests on model grouted pile shafts in uncemented calcareous sediment have revealed the following trends :

(1) For normally consolidated sand, the skin friction, f_s, increases with effective overburden pressure σ'_{vo}. The ratio of f_s/σ'_{vo} is of the order of 0.75 to 1.0 in dense sand for σ'_{vo} less or equal to 200 kPa; this ratio is significantly higher than the value for jacked piles.

(2) The ratio f_s/σ'_{vo} increases with increasing over-consolidation ratio and with increasing relative density.

(3) The soil modulus, E'_{50}, increases as σ'_{vo} increases and the ratio E'_{50}/σ'_{vo} also increases with increasing OCR. However, the relative density of the sand appears to have little effect on the values of E'_{50} and E'_{50}/σ'_{vo}.

(4) The cyclic degradation of skin friction is greatly influenced by the cyclic displacement. At large cyclic displacements, the skin friction may be reduced to as little as 5% of its initial value.

(5) The major factor controlling cyclic degradation of skin friction appears to be the cyclic slip displacement. When compared on this basis, test data from two different types of tests are consistent with the present data on cyclic degradation.

(6) A cyclic stability diagram provides a meaningful way of describing the response of pile subjected to various combinations of mean and cyclic load levels. For the model pile tests, two distinct zones are clearly defined : a stable zone in which cyclic loading causes no reduction in load capacity, and an unstable zone in which the pile will fail during cyclic loading within a specified number of cycles. These results are consistent with data from other field tests.

(7) "Fatigue curves", representing the relationship between cyclic load level and number of cycles to failure, indicate that the latter can be very sensitive to cyclic load level, and that the mean load level is also a significant factor.

(8) The general observed characteristics of the cyclic stability diagrams and fatigue curves" of the pile can be simulated reasonably well by a simple analysis based on a simple skin friction degradation model.

The model test data clearly demonstrates that, while grouted piles in calcareous sediments may develop substantial skin friction under static loading, there is the potential for significant loss of shaft load capacity if the cyclic load level exceeds about 20% of the static shaft load capacity.

ACKNOWLEDGEMENTS

REFERENCES

DEANE, R., SHADE, D., SCHRIER, W. & WILLIAMS, A.F. (1988). Development and Implementation of Grouted Section Tests. Int. Conf. on Calcareous Sediments, Vol. 2, pp. 485-492.

DIYALJEE, V.A. & RAYMOND, G.P. (1982). Repetitive Load Deformation of Cohesionless Soil. Jnl. Geot. Eng. Divn., ASCE, Vol. 108, No. GT10, pp. 1215-1229.

HULL, T.S., POULOS, H.G. & ALEHOSSEIN, H. (1988). The Static Behaviour of Various Calcareous Sediments. Int. Conf. on Calcareous Sediments, Vol. 1, pp. 87-96.

JOHNSTON, I.W., CARTER, J.P., NOVELLO E.A. & OOI, L.H. (1988). Constant Normal Stiffness Direct Shear Testing of Calcarenite. Int. Conf. on Calcareous Sediments. Vol. 2, pp. 541-554.

LU, B.T.D. (1986). Axial Behaviour and Capacity of Driven Piles in Calcareous Sands. 18th Annual Offshore Tech. Conf., Paper OTC 5148, pp. 579-588.

MATLOCK, H. & FOO, S.C. (1979). Axial Analysis of a Pile Using a Hysteretic and Degrading Soil Model. Proc. Int. Conf. on Numerical Methods in Offshore Piling, London, I.C.E., pp. 165-185.

MURFF, J.D. (1987). Pile Capacity in Calcareous Sands : State of the Art. Journal of Geot. Eng. Divn., ASCE, Vol. 113, No. 5, pp. 490-507.

NAUROY, J.F., BRUCY, F. & LE TIRANT, P. (1985a). Static and Cyclic Load Tests on a Drilled and Grouted Pile in Calcareous Sand. BOSS 85, Delft. pp. 577-587.

NAUROY, J.F. & LeTIRANT P. (1985b). Driven Piles and Drilled and Grouted Piles in Calcareous Sands. Offshore Technology Conference, Paper OTC 4850, pp. 83-91.

POULOS, H.G. (1988). Cyclic Stability Diagram for Axially Loaded Piles. Jnl. Geot. Eng. Divn., ASCE, Vol. 114, No. 8, pp. 877-895.

POULOS, H.G. (1989). Cyclic Axial Loading Analysis of Piles in Sand. Jnl. Geot. Eng. Divn., ASCE, Vol. 115, No. 6, pp. 836-852.

POULOS, H.G. & CHAN, K. (1986). Laboratory Study of Pile Skin Friction in Calcareous Sand. Geot. Eng., Vol. 17, No. 2, pp. 235-237.

POULOS, H.G. & LEE, C.Y. (1988). Model Test on Grouted Piles in Calcareous Sediment. Int. Conf. on Calcareous Sediments, Perth, Vol. 1, pp. 255-260.

POULOS, H.G. & LEE, C.Y. (1989). Behaviour of Grouted Piles in Offshore Cal-

careous Sand. Proc. of 12th Int. Conf. on Soil Mechanics and Foundation Eng., Rio de Janeiro, pp. 955-958.

RANDOLPH, M.F. & WROTH, C.P. (1978). Analyses of Deformation of Vertically Loaded Piles. Jnl. Geot. Eng. Divn., ASCE, Vol. 104, No. GT12, pp. 1465-1488.

YOUNG, G.S. (1983). Investigation of Axial Cyclic Loading of Model Piles in Calcareous Sand. M. Eng. Sc. Thesis, The University of Sydney.

APPENDIX

NOTATION

A	permanent displacement parameter
D_τ	degradation factor for skin friction
$D_{\tau lim}$	minimum possible value of D_τ
D_r	relative density of soil
d	pile shaft diameter
E_s	Young's modulus of soil
E'_{max}	drained value of E_s for low stress levels
E'_{50}	drained value of E_s for 50% stress level
f_c	skin friction after cyclic loading
f_s	skin friction for static loading
m, n	permanent displacement parameters
N	number of cycles
N_f	number of cycles to cause failure
OCK	overconsolidation ratio
P_c	cyclic load
P_o	mean load
P_u	static ultimate load capacity
S_p	permanent displacement of pile
ϕ	drained friction angle of soil
λ	degradation rate parameter
ν_s	Poisson's ratio of soil
ν'_{min}	drained value of ν_s for low stress levels
ρ_c	cyclic displacement
ρ_{fs}	displacement to cause static pile-soil slip
σ'_c	effective confining pressure in triaxial test
σ'_{vo}	effective surcharge (overburden) pressure in pile test.